

Additive manufacturing of Lunar Regolith Simulant using Direct Ink Writing

Billy Grundström [1], **Timon Schild** [2], **Aidan Cowley** [1]

[1] *Uppsala University*
Uppsala, Sweden

[2] *ESA/EAC - European Astronaut Centre*
Cologne, Germany

[3] *European Space Agency - ESA*
Cologne, Germany

Abstract

This work explores the use of a lunar regolith simulant as feedstock for the direct ink writing additive manufacturing process as an option to enable future lunar in-situ resource utilisation. The feasibility of this approach is demonstrated in a laboratory setting by manufacturing objects with different geometries, using methyl cellulose or sodium alginate as binding agents, water and lunar regolith simulant to create a viscous, printable 'ink'. A custom three-axis gantry system is used to produce green bodies for subsequent sintering. The sintered objects are characterised using compressive strength measurements and scanning electron microscopy (SEM). It is proposed that the bioorganic compounds used in this work as additives could be produced in situ for a future lunar base through photosynthesis, utilising carbon dioxide exhaled by astronauts together with the available sunlight. Thus, all the components used for the dispersion – additive, water, and regolith – are available in situ. The compressive strength for sintered samples produced with this method was measured to be 2.4 MPa with a standard deviation of 0.2 MPa ($n = 4$). It is believed, based on the high sample porosity observed during SEM analysis, that the comparatively low mechanical strength of the samples is due to a low sintering temperature, and that the mechanical strength could be increased by optimising the sintering process further.

Keywords

ISRU, additive manufacturing, 3D printing, direct ink writing, lunar regolith, sintering

DOI

<https://doi.org/10.7480/spool.2021.2.5268>

Context

A limiting factor for human space exploration is the restricted amount of mass that can be transported into space due to the high cost of space travel (Anand et al., 2012). Even though this cost is expected to decrease with the further development of reusable launch systems, the cost per transported mass is likely to remain high due to intrinsic limitations in the storage capacity of spacecraft related to the required propulsion mass (Sherwood, 2019) "ISSN": "00945765"; "abstract": "NASA planning for the human space flight frontier is coming into alignment with the goals of other planetary-capable national space agencies and independent commercial actors. US Space Policy Directive 1 made this shift explicit: "the United States will lead the return of humans to the Moon for long-term exploration and utilization". The stage is now set for public and private American investment in a wide range of lunar activities. Assumptions about Moon base architectures and operations are likely to drive the invention of requirements that will in turn govern development of systems, commercial-services purchase agreements, and priorities for technology investment. Yet some fundamental architecture-shaping lessons already captured in the literature are not clearly being used as drivers, and remain absent from typical treatments of lunar base concepts. A prime example is general failure to recognize that most of the time (i.e., before and between intermittent human occupancy. The cost associated with sending one pound – approximately 0.45 kg – of mass into orbit has been estimated to be at least \$10,000 (Montes et al., 2015).

In-situ resource utilisation (ISRU) is a methodology for reducing the amount of material needed to be sent from Earth by using resources available at the destination during coming missions to the Moon or to Mars. Such an example of ISRU is the planned demonstration of oxygen production from atmospheric CO₂ by the Mars rover Perseverance, launched in 2020 by the National Aeronautics and Space Administration (NASA) (Hinterman, 2020). Another example would be the use of native construction materials for buildings and infrastructure on the Moon or on Mars. One such material that has attracted significant interest in the context of space exploration is regolith, which is an umbrella term for the compositionally and morphologically heterogeneous surface layer of rock and fine particles on celestial bodies. The use of regolith has been studied extensively for ISRU applications (Anand et al., 2012; Nieke et al., 2019; Schleppe et al., 2019; Sherwood, 2019; Song et al., 2019).

Additive manufacturing (AM) – or three-dimensional (3D) printing – is a manufacturing process that has raised much interest in the last couple of decades. This is due to its ability for rapid prototyping as well as the high level of design freedom enabled by the technology compared to traditional subtractive manufacturing (SM) technologies. These and other features makes AM an attractive technology for future ISRU applications in remote locations (Jakus et al., 2015; Schlordt et al., 2013; Taylor et al., 2017). During the AM process, an object is built in a layer-by-layer fashion. There exists a multitude of different AM technologies, spanning the material categories of ceramic, metallic, and polymer materials (ISO/ASTM, 2015).

Direct ink writing (DIW) – or robocasting – is an AM technology that is based on the selective deposition of a viscous ink by extrusion through a nozzle (Lewis et al., 2006) functional, and biomedical applications. One facile approach is direct ink writing (DIW). The ink (also called dispersion or slurry) usually consists of solid particles dispersed in a liquid phase, and is typically optimised with regards to its rheological properties by the use of additives, especially by modifying the ink to have it exhibit shear thinning behaviour for facilitated deposition (Dai et al., 2019). Additional additives may be used to further optimise the properties of the ink such as controlling the flocculation behaviour of the particles. Typical factors to consider when choosing the liquid phase for the ink are availability, its rate of evaporation, as well as its toxicity. Depending on the final use, the 3D-printed item, once manufactured, might be further processed, for example by sintering.

Combining additive manufacturing with ISRU is an attractive option, as a single technological system might be used to manufacture objects with differing geometries for a wide range of applications. Table 1 summarises published articles on the use of regolith as a material for additive manufacturing, as well as a minor selection of articles in which casting is used as a production method. It should be noted that test conditions (e.g. geometries, number of replicates, and the standards used) for the performed compressive strength measurements vary between sources, which in effect makes a direct comparison of the results of limited use. Still, the compressive strength has been included in the table to give a sense of the current state of each technology. It should also be noted that the availability of actual lunar regolith is highly limited. Therefore, research relating to this topic almost exclusively makes use of regolith simulants of terrestrial origin, the choice of which may affect the results.

METHOD	SUBPROCESS	MATERIAL	COMPRESSIVE STRENGTH	REFERENCE
AM	Binder jetting	Regolith, Sorel cement, binder liquid	20 MPa	(Cesaretti et al., 2014)
AM	Extrusion	Regolith (72 wt.%), urea, alkaline solution, Casted	13 MPa	(Pilehvar et al., 2020)
AM	Extrusion	Regolith (56 wt.%), phosphoric acid, water, Machined	20 MPa	(Buchner et al., 2018)
AM	Extrusion	Regolith (74 vol.%), PLGA, DCM, plasticizer	19 MPa	(Taylor et al., 2018)
AM	Extrusion	Regolith (70 vol.%), PLGA, DCM, plasticizer	Not tested	(Jakus et al., 2017)
AM	Laser melting	Regolith	31 MPa	(Caprio et al., 2020)
AM	Laser melting	Regolith	Not tested	(Goulas et al., 2016)
AM	Laser sintering	Regolith	Not tested	(Xu et al., 2019)
AM	Laser sintering	Regolith	Not tested	(Goulas & Friel, 2016)
AM	Laser sintering	Regolith	Not tested	(Fateri & Gebhardt, 2015)
AM	Laser sintering	Regolith	Not tested	(Balla et al., 2012)
AM	Microwave sintering	Regolith	Not tested	(Allan et al., 2013)
AM	Solar sintering	Regolith	2 MPa	(Meurisse et al., 2018)
Casting	Geopolymer	Regolith (76 wt.%), liquid silicate, alkaline solution	16 MPa	(Montes et al., 2015)
Casting	Sulphur concrete	Regolith (65 wt.%), sulphur	31 MPa	(Toutanji et al., 2012)
Casting	Thermite reaction	Regolith (67 wt.%), aluminium powder	18 MPa	(Faierson et al., 2010)

TABLE 1 Overview of reported use of regolith together with mainly additive manufacturing processes.

Innovation

This work focuses on the use of an extrusion-based additive manufacturing technology – direct ink writing – using a formulation that is both non-toxic and easy to produce in situ. Indeed, the current extrusion-based processes described in the literature often use additives that are hazardous (e.g. DCM, phosphoric acid) and/or difficult to produce in situ (e.g. plasticizers). The selection criteria for the proposed formulation were in this instance, in descending order, low toxicity, potential in-situ availability, and low technological complexity in order to increase the robustness of the system.

Water was chosen as the liquid phase owing to its non-toxicity and potential availability on the Moon (Colaprete et al., 2010). Sodium alginate (SA) and methyl cellulose (MC), two bioorganic compounds, were both identified as suitable binding agents for the dispersion. A scenario is envisioned here in which either sodium alginate or methyl cellulose is produced in situ on the Moon by the use of microorganisms and bioreactors, utilising CO₂ exhaled by astronauts (Menezes et al., 2015; Way et al., 2011) all of which can be

generated by means of biosynthesis. Synthetic biology has the potential to generate organisms designed for supplying human nutritional needs in space. Photosynthetic microbes may be ideal for this purpose, as they are more efficient per volume cultivated than green plants at conversion of light to chemical energy, biomass and nutritional molecules. In addition, microbes are easier and faster to genetically engineer, facilitating not only design and terrestrial manufacture of organisms optimized for growth and nutrient production in the artificial conditions of space, but superior ability in space to develop organisms suited to newly discovered environments. The rapid ability to adapt and create new microbes to suit new circumstances when in space offers significant potential for risk reduction. Development of sun-driven microbial production of nutritional chemicals would also have terrestrial benefits in commerce and sustainability. A synthetic biology approach to chemical production would not be based on fossil fuels as such fuels do not exist on other planets. This approach would highlight a synergistic relationship between outer space and 'spaceship earth', illustrating NASA's role in stimulating technology development with terrestrial application. Two specific approaches deserve consideration: production by traditional photosynthetic microbes, or by the newly appreciated capacity of some bacteria to absorb electric current (e.g. solar panels). In such a scenario, all the ingredients for the dispersion – regolith, water, and binding agent – could be sourced locally once the initial infrastructure has been installed.

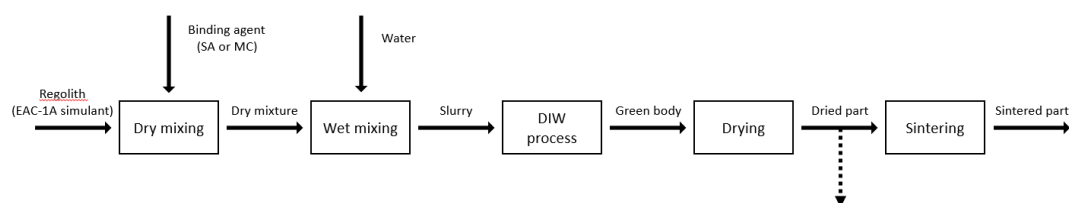


FIGURE 1 Proposed process for 3D parts production using regolith slurry.

A schematic of the proposed process is presented in Figure 1. The regolith (i.e. EAC-1A simulant) is first mixed with the powdered binding agent (SA or MC) to form a dry mixture. A slurry is then produced by addition of deionized water and thorough mixing. This slurry is a viscous fluid loaded in regolith, which can be used for DIW. A 3D-printing rig is used to extrude the slurry on a build-plate and produce a 3D geometry. The printed green body is air-dried to obtain a dried part, which can be used as is or sintered in a furnace to obtain the final sintered part.

In this paper, the feasibility of the proposed process is demonstrated through experimental results. A working set of process parameters is established, and the properties of the produced parts are assessed.

Experimental methods

Materials

EAC-1A, a lunar regolith simulant developed by ESA, was used for this work. It is readily available and has been shown to be comparable to other frequently used regolith simulants (Engelschiøn et al., 2020). The material composition in wt.% as reported in the literature is summarised in Table 2. The grain size for

the material ranges between 0.02–1.0 mm. In terms of granulometry, EAC-1A mostly falls within the range of values observed in Apollo samples, with a slight underrepresentation of particles between 200 µm and 70 µm. The elemental composition of EAC-1A is closest to the one observed in the Apollo 17 samples.

EAC-1A, as any other regolith simulant, does differ from actual lunar regolith in a few aspects relevant to this work. First of all, lunar regolith grains have very irregular shapes, and are often elongated with sharp edges and corners. As a terrestrial simulant, EAC-1A displays more rounded grain shapes. This may affect the mechanical properties of the slurry, such as its flowability or its cohesion strength. Actual lunar regolith also has a large glass fraction (up to 60%wt), which is difficult to reproduce in terrestrial simulants. The absence of this glass phase in EAC-1A could affect the sintering behaviour of the produced green bodies.

OXIDE	WT.%
SiO ₂	43.70
Al ₂ O ₃	12.60
Fe ₂ O ₃	12.00
MgO	11.90
CaO	10.80
Na ₂ O	2.90
TiO ₂	2.40
K ₂ O	1.30
P ₂ O ₅	0.60
MnO	0.20
Total	98.40

TABLE 2 Chemical composition of the lunar regolith simulant EAC-1A in wt.%.

Two dispersions were prepared by mixing ingredients according to the ratios given in Table 3, with 'LA' referring to 'Low Additive' content and 'HA' referring to 'High Additive' content respectively. HA samples had an increased concentration of additive by a factor of 3.6. Dispersions were prepared using either methyl cellulose (MM = 160000 g/mol) or sodium alginate (both Carl Roth GmbH + Co. KG, Germany) as additives. EAC-1A regolith simulant was mixed with the powdered additive, to which de-ionised water was then added. The mixture was hand stirred for at least 5 minutes using a mortar and pestle. The resulting dispersion was transferred to a 60 ml syringe for immediate use. After finishing a print, the resulting items were left to dry under ambient atmospheric conditions for 72 h before sintering.

	EAC-1A	WATER	ADDITIVE
LA	1	0.40	5.6 · 10 ⁻³
HA	1	0.45	2.0 · 10 ⁻²

TABLE 3 Dispersion content as component mass/EAC-1A mass ratio. (LA: Low Additive, HA: High Additive).

3D printing

An overview of the key components of the 3D printer used in this work is given in Figure 2. It is a 3-axis system, allowing a custom slurry extruder to be moved along the X,Y, and Z directions over a fixed printed bed. The custom unit is controlled through a controller board which has a graphical user interface and that runs a

modified version of the Marlin firmware. The X- and Y-axes (lateral axes) are belt driven by stepper motors connected to microstep drivers for current regulation and step size control. The Z-axis (vertical axis) is a rack and pinion system driven by a stepper motor, on which the extruder subunit can be mounted. The extruder has a stepper motor which actuates a leadscrew with a custom plunger attached to its end that fits into a 60 ml syringe with a 28 mm chamber diameter. The 3D printer takes G-code files as input. The movement speed for the X- and Y-axes was set to 7 mm/s and the extrusion speed was set to 4 μm per mm X and Y travel, which corresponds to 28 $\mu\text{m}/\text{s}$ or a volumetric flow of 17 mm^3/s . The system parameters of importance are listed in Table 4.

To perform the printing operation, the slurry is loaded into the extruder syringe and deposited onto an unheated ceramics buildplate. Since the slurry formulations used were subject to air-drying, the printing operation was undertaken within 30 minutes after slurry production. After printing, the parts were left on the printbed to dry at room temperature for at least 72 hours. This allowed the sample to build enough strength to be separated from the printbed for further processing without damaging the geometry.

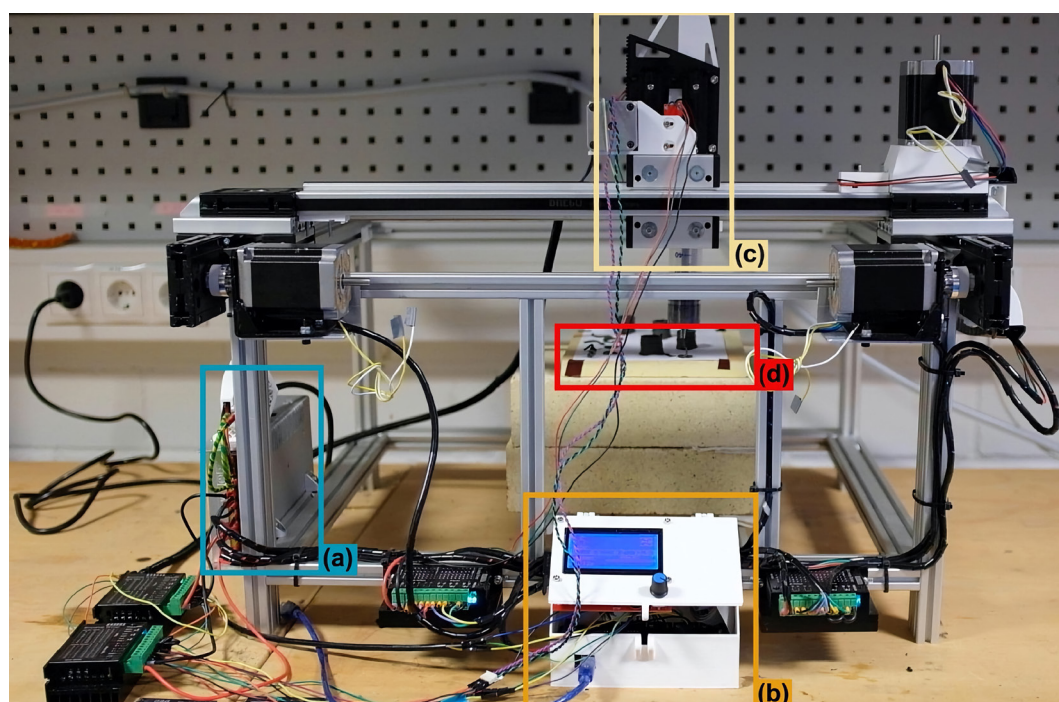


FIGURE 2 Custom 3D printer overview: (a) power supply unit, (b) controller board with SD slot and graphical user interface, (c) Z-axis and extruder, (d) ceramic build plate.

SYRINGE VOLUME	NOZZLE DIAMETER	X, Y MOVEMENT SPEED	EXTRUSION SPEED	VOLUMETRIC FLOW	LAYER HEIGHT
60 ml	2 mm	7 mm/s	28 $\mu\text{m}/\text{s}$	17 mm^3/s	1.2 mm

TABLE 4 System parameters for the custom 3D printer.

Sintering

The sintering was carried out using a Paragon SC-Series 1680 W Kiln with a specified max. temperature of 1093 $^{\circ}\text{C}$, with an actual max. temperature varying around 1080 $^{\circ}\text{C}$ during sintering. The sintering was carried out over three steps, listed in Table 5, and the kiln was then left to cool to room temperature over a period of approximately 2 h. The total process took approximately 8.5 h from start to finish.

STEP	TARGET TEMPERATURE	HEATING RATE	HOLDING TIME
Drying	120 °C	5 K/min	45 min
Debinding	500 °C	5 K/min	45 min
Sintering	1080 °C	10 K/min	120 min

TABLE 5 Sintering steps.

Characterisation

A Hitachi TM-1000 scanning electron microscope with an accelerating voltage of 15.0 kV was used for this work. A Shimadzu AGX universal testing machine with a force accuracy of $\pm 0.5\%$ was used at a speed setting of 1 mm/min for the compressive testing.

Results and discussion

Slurry preparation

When only regolith and water are mixed, the mixture separates into its solid and liquid components as regolith lacks the cohesiveness of clay materials, meaning that water itself is not sufficient to create a self-supporting and extrudable slurry. By using methyl cellulose or sodium alginate as a binding agent, the viscosity of the dispersion is markedly increased as the additive comes in contact with water. The dispersion may be modified from being water-like with high flowability, to being a thick, nonflowing paste, by altering the concentration of additive. Both SA and MC behaved in similar way in this study. In a shear thinning liquid, such as one that is ideally used for 3D-printing applications, an increase in the strain rate will lead to a decrease in viscosity. Both SA and MC slurries reportedly exhibit this behaviour (Liu et al., 2018; Schlördt et al., 2013).

There was an observed increase in rigidity of an extruded strand of dispersion during this work as the concentration of additive was increased. An extruded segment of the higher additive 'HA' concentration dispersion resisted attempts at indentation with a sharp object, while the lower additive 'LA' concentration did not do so. It is possible that this increase in observed rigidity counteracts the interaction and bonding between subsequent layers. This might increase anisotropy in the material due to the reduced bonding strength between layers, similar to what is commonly observed in thermoplastic 3D printing (Hart et al., 2018). As a result, it is suggested that a higher concentration of additive will result in weaker structures if a certain threshold value of additive is surpassed due to reduced layer bonding.

Mixing is an important step to ensure a well dispersed slurry, and the use of a ball mill instead of mortar and pestle might improve the distribution and dispersion of particles in the slurry. At higher concentrations of additive, it was difficult to manually homogenise the slurry, as the material had the viscosity of a thick paste. It has been suggested elsewhere that the ratio of nozzle size to maximum particle diameter should be 10, which equals particles with a maximum size of 200 μm for a 2 mm nozzle, like the one used here (Perrot et al., 2018). As already mentioned, the particles used in this work ranged between 0.02 and 1 mm in diameter (before mixing), which might lead to non-optimal flow behaviour.

3D printing

The prepared dispersions proved to be extrudable using the 3D printer system available for this work. A selection of parts printed using this setup are presented in Figure 3.

Experiments using higher concentrations of additive than those reported here were also conducted, but extrusion was no longer possible due to the limitations of the setup. Similarly, tests were performed using finer nozzle sizes (0.8 mm and 1.2 mm) in combination with the sieved fraction EAC-1A, with the result that the system again was not able to extrude the dispersion. This indicates that an upgraded setup with higher extruding pressure may help improve the process. Indeed, the feature size of printed items depends on the nozzle size, meaning that a finer nozzle enables higher resolution.

It is also important that the printed items exhibit a high green strength to support the subsequent layers as they are deposited. Figure 3 (a) displays a printed hollow cylinder that is approximately 20 mm tall, consisting of 15 layers, in which SA was used at a low concentration ('LA'). This object demonstrates that the prepared dispersion has enough shape retention to carry its own weight at this scale. The cylinder is not perfectly straight, but it is not certain if this is due to self-buckling of the structure, small inaccuracies in the movement of the printhead, or to slight deviations in how the dispersion expands and contracts after extrusion, which, as the print progresses, may lead to dimensional inconsistencies.

It has been reported that a difference of only 2 vol.% in solid loading for a ceramic dispersion can have a significant impact on the buckling behaviour of the ink (Rueschhoff et al., 2016; Tang et al., 2019), which may be an important consideration when seeking to avoid any self-buckling tendencies of the ink.

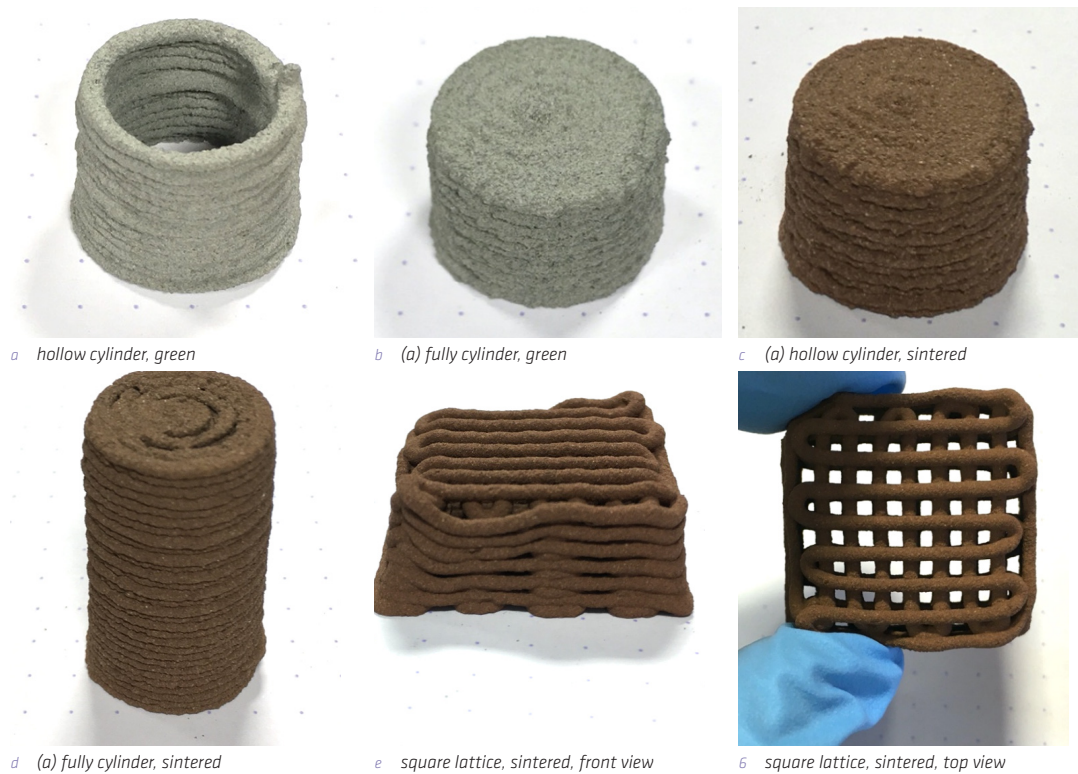


FIGURE 3 Parts produced by direct ink writing of regolith simulant slurry (distance between the dots is 10 mm)

Figure 3 (e) & (f) shows a 3D printed lattice structure after sintering, the dispersion used being low additive ('LA') with SA as a binder. It can be seen that the structure has collapsed at the unsupported sections, creating a defect along the side that progressively worsens. However, this collapse had little influence on the actual inner grid structure, which retained its shape relatively well, as seen in the figure. It should be noted that for the commonly used thermoplastic fused filament fabrication (FFF) process, overhangs exceeding 45° are generally not printed without the use of a support structure, and it should therefore not be surprising to observe that the dispersion used here is unable to support 90° overhangs. If a finer grid had been printed, it is possible that the structure would be able to support itself, as can already be observed in certain places.

Figure 3 (d) depicts a 3D-printed cylinder that is 33.8 mm tall created with the 'LA' dispersion using SA. As demonstrated by this structure, solid objects exhibit structural integrity both during and after printing. The gaps seen at the top are believed to be due to dispersion shrinkage after deposition as water evaporates. A way to compensate for this would be to use a line width during printing that is slightly less than the nozzle diameter, e.g. 1.8–1.9 mm instead of the 2 mm used here.

An observation when using the 'HA' concentration of sodium alginate to print a set of rectangular objects was that a crack evolved in all the objects along the same direction on the underside that was in contact with the ceramic build plate. These cracks were noticed after the drying period of 72 h, and it is therefore not known when they developed as the underside of the samples were not visible until the objects were turned, but this is likely due to the drying process.

A possible explanation for this behaviour is that the outer surface of the objects dries at a higher rate than the inside of the objects. As water evaporates, the volume of the item will decrease, and this shrinkage will be more pronounced at the outer edges of the samples. If the object is relatively stiff, as noticed when using the 'HA' concentration, the parts of the sample with a less pronounced shrinkage (i.e., the inner regions) will 'resist' this shrinkage, and the tension arising in the sample will give rise to the observed crack. No cracks were observed in samples prepared using the 'LA' concentration, and it is believed that the reduced stiffness or rigidity of the 'LA' concentration creates less build-up of tension in the samples during the drying process compared to the 'HA' concentration, or that the tension is more easily dissipated in the 'LA' concentration samples. Another explanation could be the difference in liquid-to-powder ratio between 'LA' and 'HA' concentrations, as this will affect the capillary action – i.e., the transport of the liquid phase – and porosity in the material. In any case, this observation suggests that there is an upper limit to the amount of additive that should be used, which is below the value at which the dispersion still shows good printability during the AM process, as was the case for the high additive concentration slurry used here.

It is likely that the direct ink writing process – due to the use of a liquid phase – inevitably will produce relatively loosely packed samples, at least when compared to other green body preparation processes such as compaction through an external force. There is a risk that this porosity will have a detrimental effect on the sintering step. This might be mitigated by reducing the non-solid mass of the slurry as much as possible, i.e., by optimising the dispersion with regards to a low water content. Still, the achievement of dense ceramic bodies has been reported for the DIW process (Rueschhoff et al., 2016).

Sintering

Figure 3 (a) & (b) show the same 3D-printed solid cylinder before and after sintering, using the 'LA' dispersion and SA as an additive. There is little observable difference between the two, with the noticeable exception of hematite formation, which takes place during sintering in an oxygen rich

environment and gives rise to the observed reddish-brown colour (Zocca et al., 2020). If regolith is sintered under oxygen-deprived conditions – e.g. vacuum – the objects retain their greyish colour (Taylor et al., 2018)“ISSN”:"00945765"“abstract”:"The development of in situ fabrication methods for the infrastructure required to support human life on the Moon is necessary due to the prohibitive cost of transporting large quantities of materials from the Earth. Cellular structures, consisting of a regular network (truss.

No significant densification of the samples was observed in this work as the items retained most of their initial volume after sintering. Small dimensional deviations in the sample made it difficult to determine its volume with a sufficient degree of accuracy when using a hand measuring tool. Otherwise, if the volume was known, it would be possible to determine the degree of densification during sintering.

A comparison that was performed of the mechanical strength between a sintered and an unsintered sample under compression with a hand tool suggests that the strength of the sintered sample is only slightly higher than that of the unsintered sample. An explanation for this could be a less-than-optimal sintering process. It might be tempting to view the colour change of the samples as a sign of successful sintering, but hematite formation is already significant at temperatures around 850 °C, well below the reported sintering start at 1091 °C for particles with a diameter of 100 µm or smaller (Zocca et al., 2020). As the sintering temperature reached for this work – 1080 °C – is less than the reported sintering start, and also considering that the grain size distribution for the samples prepared in this work range between 20–1000 µm, i.e. containing particles larger than 100 µm, it is reasonable to believe that the sintering was limited in its effect, if it even took place at all.

The heat rate of the sintering protocol (not only the temperature) is also expected to influence the mechanical properties of the sintered objects. Here, a heat rate of 5 K/min was chosen for the initial drying and debinding steps. The choice of this heat rate was motivated by reported heat rates for sintering of regolith material found in the literature (Taylor et al., 2018; Zocca et al., 2020)“ISSN”:"00945765"“abstract”:"The development of in situ fabrication methods for the infrastructure required to support human life on the Moon is necessary due to the prohibitive cost of transporting large quantities of materials from the Earth. Cellular structures, consisting of a regular network (truss. Decreasing the heat rate during sintering will allow for a more uniform heating and cooling of the object, which in turn reduces the risk of crack formation during sintering due to temperature gradients in the material. It might be beneficial to the mechanical strength of the objects to reduce the heat rate even further than was done in this work, although there is likely to be a trade-off between mechanical strength and considerations associated with an increased processing time such as cost and practicability.

It should also be expected that the complex mineralogy found within regolith will give rise to complex melting behaviour (Meurisse et al., 2017). Certain minerals – or additives – in the material, having different melting temperatures than that of the rest of the matrix, could give rise to liquid phase sintering of the material. This in turn might facilitate the densification of a porous sample, as the liquid phase is able to penetrate voids in the sample.

SEM

The SEM analysis was performed on the cross section of a sintered rectangular sample manufactured using the 'LA' concentration of sodium alginate. The images obtained at magnifications of x100, x500, and x1000 can be seen in Figure 4. Figure 4 (a) displays a low magnification image of the sample, illustrating the heterogeneous nature of the material, with particles visible in a variety of shapes and sizes, the largest of

them appearing to be about 200 μm . As mentioned previously, the EAC-1A feedstock material used has a grain size range of 0.02-1.0 mm. The apparent absence of $>200 \mu\text{m}$ grains can be explained by the grinding that occurs during slurry preparation, done with a pestle and mortar. It is proposed that this leads to the 0.2-1.0 mm grains being broken down into smaller grains $<200 \mu\text{m}$.

We also observe high porosity in the sample, which can further be seen in Figure 4 (b), taken at a higher magnification. Again, a large spread in particle sizes and shapes is observed, and the sample may be classified as being highly porous due to the significant amount of void space between particles, as seen in the figure. It is possible that a finer particle size of the material than that used here would allow a higher degree of close packing of particles, which in turn would facilitate sintering as discussed previously. Furthermore, an increase in solid phase during slurry preparation – i.e. a reduced water content – might lead to a denser sample, as the void volume that is observed here is likely to previously have been occupied by the gel-phase that is evaporated during the drying and sintering stages.

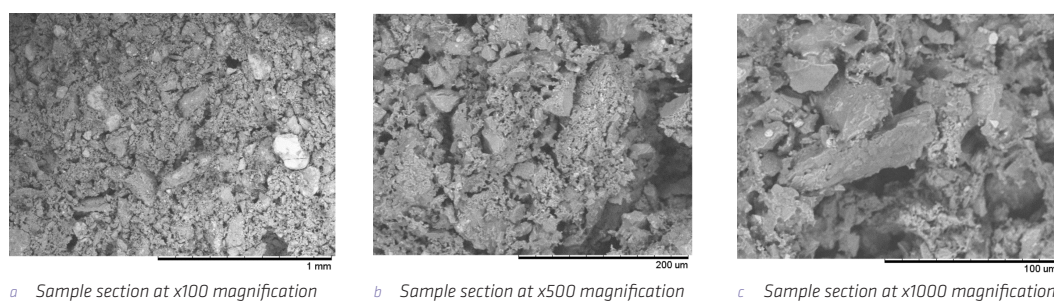


FIGURE 4 SEM analysis of sintered 'LA' sample produced by DIW.

In Figure 4 (c), jagged particle shapes can be observed throughout the sample; it is not clear whether this is a result of the slurry preparation step, or a property of the stock material, even though it is reasonable to believe that the pestling during the slurry preparation would influence particle morphology. The average sphericity F for the material has been reported as being in the range 0.59–0.60 F , where a sphere equals unity, indicating a moderate sphericity for the stock material (Engelschiøn et al., 2020).

Compression testing

Sintered solid cylinder samples such as the one shown in Figure 3 (a) & (b) above were used for compression testing. Four samples with an average diameter of 18.5 mm and an average height of 14.6 mm were tested. During the initial phase of the test, the load was concentrated on surface irregularities on the top of the samples; as these gave way, the load was spread evenly over the top surface of the cylinder. Before reaching the recorded maximum load of each test, cracks were observed that propagated throughout the samples. An example of a force/displacement curve obtained is shown in Figure 5.

The average value for the compressive strength of the samples was recorded to be 2.4 Mpa, with a standard deviation of 0.2 MPa. Compared with the values in Table 1, the compressive strength in this work is about one order of magnitude less than what is commonly reported. As discussed previously, it is believed that less-than-optimal sintering was achieved during our experiments, which would explain the low value for compressive strength.

An average value for the Young's modulus of the samples was calculated to be 36.8 MPa, with a standard deviation of 10.9 MPa. This value was calculated from the measured peak force and associated displacement at the end of the linear region of the plot. However, this value is not believed to be an accurate representation of the material's Young modulus. Indeed, it is proposed that the linear region of the plot does not correspond to an elastic compression of the sample (associated with Young's modulus), but is due to the progressive compaction of the sample through local rupture of the weak inter-grain links. This mechanism explains the low value obtained, as well as the discontinuities that can be observed in the linear region, resulting from non-homogenous compaction of the sample.

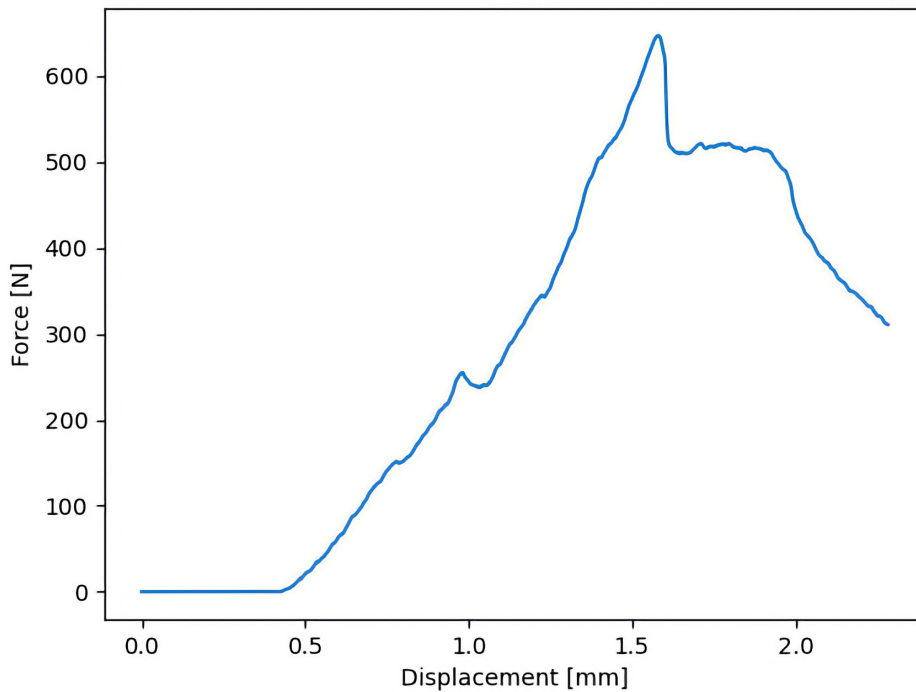


FIGURE 5 Force vs displacement curve measured during compressive testing of sample 2.

Conclusions

A new approach to additive manufacturing using regolith simulant as feedstock in the form of the direct ink writing process was proposed, in which an extrudable dispersion is prepared with regolith simulant, water, and a binding additive. Two such binding additives were identified – sodium alginate and methyl cellulose – and the feasibility of the DIW process was demonstrated through the manufacture of objects with varying geometries.

The compressive strength for sintered samples produced with this method was measured to be 2.4 MPa with a standard deviation of 0.2 MPa ($n = 4$), which is about one order of magnitude less than what is typically reported in the literature. It is believed that a non-ideal sintering process was carried out in this work. This is supported by the results from the SEM analysis, showing a highly porous inner structure of the sintered samples.

The main advantage of the proposed process is that it only uses resources which can be produced in situ on the lunar surface. Regolith and water can be sourced locally, while the additives can be produced in bio-reactors. Furthermore, the proposed process only requires a small amount of additives (about 1 wt.%) and only uses non-toxic additives.

The comparatively low compressive strength observed for the parts produced with this process limits its usefulness for manufacturing structures or functional parts. However, there are applications that could benefit from the ability of the produced parts to maintain their shape while being relatively fragile. A good example of this would be mould production for metal casting in a lunar environment. Using the presented approach, complex and diverse mould geometries could be printed on-demand using only local resources. Those moulds could then be used to produce casted metal parts, for example from recycled aluminium.

The next steps to develop this process further will focus on increasing both the compressive strength and geometrical accuracy of the parts produced. Optimizing the sintering procedure in terms of temperatures and durations should allow for more complete sintering and therefore higher mechanical strength. In addition, improving the extrusion parameters, such as the extrusion pressure and positioning accuracy, should allow the green bodies to have more precise and finer geometrical features. This could also increase the density of the green bodies, leading again to improved sintering behaviour.

References

- Allan, S., Braunstein, J., Baranova, I., Vandervoort, N., Fall, M., & Shulman, H. (2013). Computational modeling and experimental microwave processing of JSC-1A lunar simulant. *Journal of Aerospace Engineering*. [https://doi.org/10.1061/\(ASCE\)AS.1943-5525.0000245](https://doi.org/10.1061/(ASCE)AS.1943-5525.0000245)
- Anand, M., Crawford, I. A., Balat-Pichelin, M., Abanades, S., Van Westrenen, W., Péraudeau, G., Jaumann, R., & Sebaldt, W. (2012). A brief review of chemical and mineralogical resources on the Moon and likely initial in situ resource utilization (ISRU) applications. *Planetary and Space Science*, *74*(1), 42–48. <https://doi.org/10.1016/j.pss.2012.08.012>
- Balla, V. K., Roberson, L. B., O'Connor, G. W., Trigwell, S., Bose, S., & Bandyopadhyay, A. (2012). First demonstration on direct laser fabrication of lunar regolith parts. *Rapid Prototyping Journal*, *18*(6), 451–457. <https://doi.org/10.1108/13552541211271992>
- Buchner, C., Pawelke, R. H., Schlauf, T., Reissner, A., & Makaya, A. (2018). A new planetary structure fabrication process using phosphoric acid. *Acta Astronautica*, *143*(June 2017), 272–284. <https://doi.org/10.1016/j.actaastro.2017.11.045>
- Caprio, L., Demir, A. G., Previtali, B., & Colosimo, B. M. (2020). Determining the feasible conditions for processing lunar regolith simulant via laser powder bed fusion. *Additive Manufacturing*, *32*(July 2019), 101029. <https://doi.org/10.1016/j.addma.2019.101029>
- Cesaretti, G., Dini, E., De Kestelier, X., Colla, V., & Pambaguian, L. (2014). Building components for an outpost on the Lunar soil by means of a novel 3D printing technology. *Acta Astronautica*, *93*, 430–450. <https://doi.org/10.1016/j.actaastro.2013.07.034>
- Colaprete, A., Schultz, P., Heldmann, J., Wooden, D., Shirley, M., Ennico, K., Hermalyn, B., Marshall, W., Ricco, A., Elphic, R. C., Goldstein, D., Summy, D., Bart, G. D., Asphaug, E., Korycansky, D., Landis, D., & Sollitt, L. (2010). Detection of water in the LCROSS ejecta plume. *Science*, *330*(6003), 463–468. <https://doi.org/10.1126/science.1186986>
- Dai, L., Cheng, T., Duan, C., Zhao, W., Zhang, W., Zou, X., Aspler, J., & Ni, Y. (2019). 3D printing using plant-derived cellulose and its derivatives: A review. *Carbohydrate Polymers*, *203*(March 2018), 71–86. <https://doi.org/10.1016/j.carbpol.2018.09.027>
- Engelschiön, V. S., Eriksson, S. R., Cowley, A., Fateri, M., Meurisse, A., Kueppers, U., & Sperl, M. (2020). EAC-1A: A novel large-volume lunar regolith simulant. *Scientific Reports*, *10*(1), 1–9. <https://doi.org/10.1038/s41598-020-62312-4>
- Faierson, E. J., Logan, K. V., Stewart, B. K., & Hunt, M. P. (2010). Demonstration of concept for fabrication of lunar physical assets utilizing lunar regolith simulant and a geothermite reaction. *Acta Astronautica*, *67*(1–2), 38–45. <https://doi.org/10.1016/j.actaastro.2009.12.006>
- Fateri, M., & Gebhardt, A. (2015). Process parameters development of selective Laser Melting of lunar regolith for on-site manufacturing applications. *International Journal of Applied Ceramic Technology*, *12*(1), 46–52. <https://doi.org/10.1111/ijac.12326>
- Goulas, A., & Friel, R. J. (2016). 3D printing with moondust. *Rapid Prototyping Journal*, *22*(6), 864–870. <https://doi.org/10.1108/RPJ-02-2015-0022>
- Goulas, A., Harris, R. A., & Friel, R. J. (2016). Additive manufacturing of physical assets by using ceramic multicomponent extra-terrestrial materials. *Additive Manufacturing*, *10*, 36–42. <https://doi.org/10.1016/j.addma.2016.02.002>
- Hart, K. R., Frketic, J. B., & Brown, J. R. (2018). Recycling meal-ready-to-eat (MRE) pouches into polymer filament for material extrusion additive manufacturing. *Additive Manufacturing*, *21*(February), 536–543. <https://doi.org/10.1016/j.addma.2018.04.011>
- Hinterman, E. (2020). Simulating oxygen production on Mars for the Mars Oxygen In-Situ Resource Utilization Experiment. *Acta Astronautica*, *170*(October 2019), 678–685. <https://doi.org/10.1016/j.actaastro.2020.02.043>
- ISO/ASTM. (2015). INTERNATIONAL STANDARD ISO / ASTM 52900 Additive manufacturing – General principles – Terminology. *International Organization for Standardization*. <https://doi.org/10.1520/ISOASTM52900-15>
- Jakus, A. E., Koube, K. D., Geisendorfer, N. R., & Shah, R. N. (2017). Robust and Elastic Lunar and Martian Structures from 3D-Printed Regolith Inks. *Scientific Reports*, *7*, 1–8. <https://doi.org/10.1038/srep44931>
- Jakus, A. E., Taylor, S. L., Geisendorfer, N. R., Dunand, D. C., & Shah, R. N. (2015). Metallic Architectures from 3D-Printed Powder-Based Liquid Inks. *Advanced Functional Materials*, *25*(45), 6985–6995. <https://doi.org/10.1002/adfm.201503921>
- Lewis, J. A., Smay, J. E., Stuecker, J., & Cesarano, J. (2006). Direct ink writing of three-dimensional ceramic structures. *Journal of the American Ceramic Society*, *89*(12), 3599–3609. <https://doi.org/10.1111/j.1551-2916.2006.01382.x>
- Liu, Q., Li, Q., Xu, S., Zheng, Q., & Cao, X. (2018). Preparation and properties of 3D printed alginate-chitosan polyion complex hydrogels for tissue engineering. *Polymers*, *10*(6). <https://doi.org/10.3390/polym10060664>
- Menezes, A. A., Cumbers, J., Hogan, J. A., & Arkin, A. P. (2015). Towards synthetic biological approaches to resource utilization on space missions. *Journal of the Royal Society Interface*, *12*(102). <https://doi.org/10.1098/rsif.2014.0715>

- Meurisse, A., Makaya, A., Willsch, C., & Sperl, M. (2018). Solar 3D printing of lunar regolith. *Acta Astronautica*, 152(September), 800–810. <https://doi.org/10.1016/j.actaastro.2018.06.063>
- Meurisse, A., Beltzung, J.C., Kolbe, M., Cowley, A., & Sperl, M. (2017). Influence of Mineral Composition on Sintering Lunar Regolith. *Journal of Aerospace Engineering*, 30. 04017014. [https://doi.org/10.1061/\(ASCE\)AS.1943-5525.0000721](https://doi.org/10.1061/(ASCE)AS.1943-5525.0000721)
- Montes, C., Broussard, K., Gongre, M., Simicevic, N., Mejia, J., Tham, J., Allouche, E., & Davis, G. (2015). Evaluation of lunar regolith geopolymer binder as a radioactive shielding material for space exploration applications. *Advances in Space Research*, 56(6), 1212–1221. <https://doi.org/10.1016/j.asr.2015.05.044>
- Nieke, P., Kita, J., Häming, M., & Moos, R. (2019). Manufacturing dense thick films of lunar regolith simulant EAC-1 at room temperature. *Materials*, 12(3). <https://doi.org/10.3390/ma12030487>
- Perrot, A., Rangeard, D., & Courteille, E. (2018). 3D printing of earth-based materials: Processing aspects. *Construction and Building Materials*, 172, 670–676. <https://doi.org/10.1016/j.conbuildmat.2018.04.017>
- Pilehvar, S., Arnhof, M., Pamies, R., Valentini, L., & Kjøniksen, A. L. (2020). Utilization of urea as an accessible superplasticizer on the moon for lunar geopolymer mixtures. *Journal of Cleaner Production*, 247. <https://doi.org/10.1016/j.jclepro.2019.119177>
- Rueschhoff, L., Costakis, W., Michie, M., Youngblood, J., & Trice, R. (2016). Additive Manufacturing of Dense Ceramic Parts via Direct Ink Writing of Aqueous Alumina Suspensions. *International Journal of Applied Ceramic Technology*, 13(5), 821–830. <https://doi.org/10.1111/ijac.12557>
- Schleppi, J., Gibbons, J., Groetsch, A., Buckman, J., Cowley, A., & Bennett, N. (2019). Manufacture of glass and mirrors from lunar regolith simulant. *Journal of Materials Science*, 54(5), 3726–3747. <https://doi.org/10.1007/s10853-018-3101-y>
- Schlördt, T., Schwanke, S., Keppner, F., Fey, T., Travitzky, N., & Greil, P. (2013). Robocasting of alumina hollow filament lattice structures. *Journal of the European Ceramic Society*, 33(15–16), 3243–3248. <https://doi.org/10.1016/j.jeurceramsoc.2013.06.001>
- Sherwood, B. (2019). Principles for a practical Moon base. *Acta Astronautica*, 160(March), 116–124. <https://doi.org/10.1016/j.actaastro.2019.04.018>
- Song, L., Xu, J., Fan, S., Tang, H., Li, X., Liu, J., & Duan, X. (2019). Vacuum sintered lunar regolith simulant: Pore-forming and thermal conductivity. *Ceramics International*, 45(3), 3627–3633. <https://doi.org/10.1016/j.ceramint.2018.11.023>
- Tang, S., Yang, L., Li, G., Liu, X., & Fan, Z. (2019). 3D printing of highly-loaded slurries via layered extrusion forming: Parameters optimization and control. *Additive Manufacturing*, 28(February), 546–553. <https://doi.org/10.1016/j.addma.2019.05.034>
- Taylor, S. L., Jakus, A. E., Koube, K. D., Ibeh, A. J., Geisendorfer, N. R., Shah, R. N., & Dunand, D. C. (2018). Sintering of micro-trusses created by extrusion-3D-printing of lunar regolith inks. *Acta Astronautica*, 143(September 2017), 1–8. <https://doi.org/10.1016/j.actaastro.2017.11.005>
- Taylor, S. L., Jakus, A. E., Shah, R. N., & Dunand, D. C. (2017). Iron and Nickel Cellular Structures by Sintering of 3D-Printed Oxide or Metallic Particle Inks. *Advanced Engineering Materials*, 19(11). <https://doi.org/10.1002/adem.201600365>
- Toutanji, H. A., Evans, S., & Grugel, R. N. (2012). Performance of lunar sulfur concrete in lunar environments. *Construction and Building Materials*, 29, 444–448. <https://doi.org/10.1016/j.conbuildmat.2011.10.041>
- Way, J. C., Silver, P. A., & Howard, R. J. (2011). Sun-driven microbial synthesis of chemicals in space. *International Journal of Astrobiology*, 10(4), 359–364. <https://doi.org/10.1017/S1473550411000218>
- Xu, J., Cao, H., Sun, X., Tang, H., Ma, H., Song, L., Li, X., Duan, X., & Liu, J. (2019). 3D printing of hypothetical brick by selective laser sintering using lunar regolith simulant and ilmenite powders. *1084208*(February 2019), 9. <https://doi.org/10.1117/12.2505911>
- Zocca, A., Fateri, M., Al-Sabbagh, D., & Günster, J. (2020). Investigation of the sintering and melting of JSC-2A lunar regolith simulant. *Ceramics International*, February, 0–1. <https://doi.org/10.1016/j.ceramint.2020.02.212>

